



Mechanisms of selective cleavage of C–O bonds in di-aryl ethers in aqueous phase



Jiayue He^a, Chen Zhao^{a,*}, Donghai Mei^b, Johannes A. Lercher^{a,b,*}

^aDepartment of Chemistry and Catalysis Research Center, Technische Universität München, Lichtenbergstraße 4, 85747 Garching, Germany

^bInstitute for Integrated Catalysis, Pacific Northwest National Laboratory, 902 Battelle Boulevard, Richland, WA 99352, USA

ARTICLE INFO

Article history:

Received 28 June 2013

Revised 11 September 2013

Accepted 18 September 2013

Keywords:

Lignin-derived ethers

DFT calculation

Selective C–O cleavage

Aqueous phase reaction

ABSTRACT

A route for cleaving the C–O aryl ether bonds of *p*-substituted H–, CH₃–, and OH– diphenyl ethers has been explored over Ni/SiO₂ catalyst at very mild conditions (393 K, 0.6 MPa). The C–O bond of diphenyl ether is cleaved by parallel hydrogenolysis and hydrolysis (hydrogenolysis combined with HO⁺ addition) on Ni. The rates as a function of H₂ pressure from 0 to 10 MPa indicate that the rate-determining step is the C–O bond cleavage on Ni surface. H⁺ atoms compete with the organic reactant for adsorption leading to a maximum in the rate with increasing H₂ pressure. In contrast to diphenyl ether, hydrogenolysis is the exclusive route for cleaving a C–O bond of di-*p*-tolyl ether to form *p*-cresol and toluene. 4,4'-Dihydroxydiphenyl ether undergoes sequential surface hydrogenolysis, first to phenol and OC₆H₄OH⁺ (adsorbed), which is then cleaved to phenol (C₆H₄OH⁺ with added H⁺) and H₂O (O⁺ with two added H⁺) in a second step. Density function theory supports the operation of this pathway. Notably, addition of H⁺ to OC₆H₄OH⁺ is less favorable than a further hydrogenolytic C–O bond cleavage. The TOFs of three diaryl ethers with Ni/SiO₂ in water follow the order 4,4'-dihydroxydiphenyl ether (69 mol mol⁻¹_{Ni Surf} h⁻¹) > diphenyl ether (26 mol mol⁻¹_{Ni Surf} h⁻¹) > di-*p*-tolyl ether (1.3 mol mol⁻¹_{Ni Surf} h⁻¹), in line with the increasing apparent activation energies, ranging from 4,4'-dihydroxydiphenyl ether (93 kJ mol⁻¹) < diphenyl ether (98 kJ mol⁻¹) < di-*p*-tolyl ether (105 kJ mol⁻¹).

© 2013 Elsevier Inc. All rights reserved.

1. Introduction

Lignin is an abundant natural bio-polymer with methoxylated C₉ phenyl-propane units that are connected by C–O and C–C bonds [1]. Since the C–C_{aryl} bond dissociation energy (BDE) in the linkage of lignin is as high as 384 kJ mol⁻¹, it is reasonable to devise a strategy to selectively cleave the much weaker C_{aryl}–O or C_{aliphatic}–O linkages (BDE: 218–314 kJ mol⁻¹) in lignin to form phenolic fragments [2–4]. The most abundant C–O bonds in lignin are α–O–4, β–O–4, 4–O–5, β–1, and 5–5 linkages [3]; however, the 4–O–5 bond (BDE: 314 kJ mol⁻¹) [4] is the strongest. Usually, diphenyl ether is selected as the simplest model compound of 4–O–5 linkage for investigating the C–O bond cleavage chemistry.

Diphenyl ether cleavage requires harsh reaction conditions, such as near- or supercritical water at high temperature 673–773 K [5,6]. Siskin et al. reported that diphenyl ether was unreactive in the aqueous phase at temperatures lower than 733 K without catalyst, but with addition of 15% phosphoric acid catalyst, diphenyl ether was hydrolyzed to 92% phenol at 588 K after three

days [7]. In a comparison, the basic environment with 15% aqueous sodium formate, a 6.6% conversion, also to phenol was achieved at 588 K for three days. With 15% Na₂CO₃ solution, the reaction rate was accelerated and resulted in 33% conversion to phenol at 733 K after 1 h [8]. We have also reported that 100% phenol selectivity was achieved by diphenyl ether conversion over solid base catalyst K₂CO₃/ZrO₂ at 673 K [9]. Penninger et al. investigated the diphenyl ether (DPE) conversion in supercritical water at temperatures of 688–753 K with different supercritical water densities [10]. At water density below 0.3 g mL⁻¹, the radical poly-condensation dominated, forming, e.g., diphenyl, phenyl–DPE, and phenoxy–diphenyl. Increasing the water density above 0.4 g mL⁻¹ forced the reaction to follow SN₁ H⁺-catalyzed ionic hydrolysis route, yielding phenol as sole product. A NaCl concentration above 3.1 wt.% in supercritical water (SCW) greatly enhanced the hydrolysis rate of DPE [11]. This suggests that charge transfer in the water cluster surrounding the ions generated H⁺ and OH⁻ ions in the outer hydration shells formed the active species for diphenyl ether hydrolysis. Rinaldi et al. investigated the solvent effect on the hydrogenolysis of diphenyl ether over Raney nickel under 5 MPa H₂ at 363 K and concluded that a higher Lewis basicity of solvent such as methanol, 1,4-dioxane, and THF suppressed hydrogenation of aromatic products and showed no effect to C–O bond hydrogenolysis [12].

* Corresponding authors. Address: Department of Chemistry and Catalysis Research Center, Technische Universität München, Lichtenbergstraße 4, 85747 Garching, Germany. Fax: +49 89 289 13544.

E-mail addresses: chenzhao@mytum.de (C. Zhao), johannes.lercher@ch.tum.de (J.A. Lercher).

Apart from the traditional homogeneous or heterogeneous acid and base catalyzed hydrolysis of diphenyl ether in high temperature water, the metal catalyzed selective hydrogenolysis of diphenyl ether is also feasible. Hartwig et al. reported that a Ni(COD)₂ complex combined with ligand SIPr·HCl and NaO^tBu can selectively cleave diphenyl ether in *m*-xylene at 393 K and 0.1 MPa H₂, attaining 99% yields of benzene and phenol after 16 h [13,14]. While the homogeneous catalyst has minimal steric constraints on interactions with lignin model compounds and allows extremely mild conditions, the TOF with the complex Ni catalyst is as low as 0.34 h⁻¹ [13]. The catalysts are also sensitive to high concentrations of water, which is ubiquitous in raw biomass. To establish a more sustainable, stable, water-tolerant, and applicable process, we have developed a supported Ni/SiO₂ catalyst to quantitatively convert diphenyl ether to benzene and cyclohexanol at 393 K and 0.6 MPa H₂ in the aqueous phase, achieving a TOF of 26 h⁻¹ [15]. By changing the catalyst to Ni/HZSM-5, we have achieved a one-pot conversion of diverse lignin-derived phenolic monomers and aryl ethers to cycloalkanes at 523 K in the aqueous phase via cascade reactions of hydrolysis, hydrogenolysis, dehydration, and hydrogenation [16]. However, the detailed mechanisms of the C–O bond cleavage of di-phenolic ethers over the heterogeneous Ni catalysts have not been established. Therefore, in this contribution, we investigate the mechanisms of C–O bond cleavage in *p*- (H-, CH₃-, OH-) substituted diphenyl ethers over SiO₂, ZrO₂, and Al₂O₃ supported Ni catalysts in the aqueous phase by investigating individual steps. Modeling using density function theory helps to elucidate the mechanism for 4,4'-dihydroxydiphenyl ether conversion.

2. Experimental section

2.1. Reagents

All chemicals were obtained from commercial suppliers: diphenyl ether (Sigma–Aldrich, >99% GC assay), di-*p*-tolyl ether (TCI Europe, >98% GC assay), 4,4'-dihydroxydiphenyl ether (TCI Europe, >98% GC assay), cyclohexyl phenyl ether (Sigma–Aldrich, >95% GC assay), *p*-cresol (TCI Europe, >99% GC assay), hydroquinone (TCI Europe, >99% GC assay), 1,4-cyclohexanediol (TCI Europe, *cis*- and *trans*-mixture, >99% GC assay), ethyl acetate (Roth, >99.9% GC assay), phenol (Sigma–Aldrich, >99% GC assay), benzene (Fluka, >99.5% GC assay), Ni(II) nitrate hexahydrate (Sigma–Aldrich, ≥98.5%), urea (Sigma–Aldrich, BioReagent), HNO₃ (Sigma–Aldrich, >65%), 5 wt.% Pd/C (Sigma–Aldrich), SiO₂ (Aerosil 200, Evonik–Degussa), H₂ (Westfalen AG, 99.999 vol%), N₂ (Westfalen AG, 99.999 vol%), synthetic air (Westfalen AG, 99.999 vol%), ultra pure water system (EASYPure II, resistivity: 18.2 MΩ cm).

2.2. Synthesis of dicyclohexyl ether

Diphenyl ether (20.0 g) and 5 wt% Pd/C (1.0 g) were loaded in a Parr reactor (series 4848, 300 mL). After the reactor was flushed with H₂ three times, the hydrogenation reaction was conducted at 423 K in the presence of 5.0 MPa H₂ (ambient temperature) for 18 h with a stirring speed of 700 rpm. The catalysts were separated from liquid phase by centrifugation, and the product was purified through distillation under vacuum. Purity: >99% (detected by GC), *M*_w: 182 g mol⁻¹, Formula: C₁₂H₂₂O. The ¹H, ¹³C, and COSY NMR spectra are displayed in Figs. S1–S3.

2.3. Catalyst characterization

Atomic absorption spectroscopy (AAS) with a UNICAM 939 AA-Spectrometer determined the content of Ni in the supported

catalysts. Transmission electron micrographs (TEM) were recorded on a JEM-2010 Jeol transmission microscope operated at 120 kV. Before TEM measurement, the samples were prepared by depositing a drop of an ultrasonicated methanol suspension of the solid material onto a carbon-coated Cu grid for TEM measurement. Scanning electron microscopy (SEM) was recorded on a JEOL 500 SEM-microscope with accelerating voltage 25 kV. The power samples were used without any pretreatment. N₂ adsorption–desorption was carried out at 77.3 K using a PMI automatic Brunauer–Emmett–Teller (BET) sorptometer. For the H₂ chemisorption measurement, the Ni catalysts were reduced under 0.1 MPa H₂ at 733 K for 4 h prior to measurement. They were activated in vacuum at 588 K for 1 h before the H₂ chemisorption and then cooled to ambient temperature. The H₂ adsorption isotherms (chemisorption and physisorption) were measured at 1–40 kPa. Following the first isotherms, the samples were outgassed at ambient temperature for 1 h to remove the physisorbed H₂, followed by measuring another adsorption isotherm (physisorption). The Ni dispersions were calculated from the difference between extrapolated intercepts of the first and second isotherms with the assumption of H:Ni atomic ratio = 1.

2.4. Preparation of Ni/SiO₂ catalyst using deposition–precipitation (DP) method

An aqueous solution (250 mL) containing Ni(NO₃)₂·6H₂O (0.14 M, 10.2 g) was first divided in two fractions. To one 50 mL portion was added urea (0.42 M, 6.3 g). The other 200 mL portion together with SiO₂ (1.1 g) and HNO₃ (65%, 0.02 M, 0.32 mL) was put into a flask thermostated at 353 K. The first part with urea was slowly added into the flask, and the suspension was rapidly heated to 363 K. After reaching 363 K, the suspension was magnetically stirred for 10 h. Then, the suspension was cooled to 298 K, and the solids were filtered and washed three times with distilled water (5/1 = water/slurry). Finally, the sample was dried at 363 K for 24 h, and calcinated in flowing air (100 mL min⁻¹) at 973 K and reduced in flowing H₂ (100 mL min⁻¹) at 733 K. The Ni/SiO₂ catalyst had a Ni content of 57 wt.% as analyzed by AAS.

2.5. Catalytic tests

In a typical experiment, the catalytic reactions were carried out in a slurry autoclave reactor with Ni/SiO₂ catalyst using H₂O as solvent at 393 K in the presence of 0.6 MPa H₂. The diphenyl ether (0.010 mol), 57 wt.% Ni/SiO₂ (0.30 g, 2.91 × 10⁻³ mol Ni), and H₂O (80 mL) were added into a Parr reactor (Series 4848, 300 mL). After the reactor was flushed with H₂ three times, the autoclave was charged with 0.6 MPa H₂ and the reactions were conducted at 393 K with a stirring speed of 700 rpm. It heats up 9 min from ambient temperature to 393 K. As H₂O remained liquid under these conditions, two phases were formed as the reaction proceeded, requiring to determine the composition of both phases by stopping the reaction at different times and analyzing the mixture. At the selected times, the reactor was quenched by ice to ambient temperature, and the organic products were extracted by ethyl acetate and analyzed by gas chromatography (GC) and GC–mass spectroscopy (GC–MS) analysis on a Shimadzu 2010 gas chromatograph with flame ionization detector and a Shimadzu QP 2010S GC–MS, both of them equipped with a HP-5 capillary column (30 m × 250 μm). The calculations of conversion and selectivity were on carbon mole basis. Conversion = (the amount of raw-material decrease during reaction/original amount) × 100%. Selectivity = (C atoms in each product/total C atoms in the products) × 100%. Internal standards (i.e., 2-isopropylphenol for the organic phase and acetone for the aqueous phase) were used to determine the product concentration and carbon balance. The carbon balance was better than 95 ± 3%. TOFs for C–O cleavage

were calculated from the formed cleaved products per mole of active site per hour. $\text{TOF} = (\text{moles of reactants cleaved}) / (\text{moles of surface Ni sites} \times \text{reaction time in hour})$.

2.6. Computational method

To gain insight in 4,4'-dihydroxydiphenyl ether conversion over the Ni/SiO₂ catalyst, periodic density functional theory (DFT) calculations were carried out using the cp2k package [17]. The SiO₂ supported Ni catalyst was modeled by a periodic Ni (1 1 1) surface slab with four atomic Ni layers. The Ni (1 1 1) surface contained 32 atoms giving 17.2640 Å and 9.9674 Å in the *x* and *y* Cartesian directions, respectively. To avoid unphysical interactions between the periodic reactive systems, a 12 Å thickness of vacuum was inserted above the surface slabs in the *z* direction. All DFT calculations employed mixed Gaussian and plane-wave basis sets. Core electrons were represented with norm-conserving Goedecker–Teter–Hutter pseudopotentials [18–20], and the valence electron wave-function was expanded in a double-zeta basis set with polarization functions [21] along with an auxiliary plane-wave basis set with an energy cutoff of 360 eV. The generalized gradient approximation exchange–correlation function of Perdew, Burke, and Enzerhof (PBE) [22] was used for all calculations. Each configuration was optimized with the Broyden–Fletcher–Goldfarb–Shanno (BGFS) algorithm with SCF convergence criteria of 1.0×10^{-8} au. To compensate the long-range van der Waals (vdW) interaction between the adsorbate and the zeolite, the DFT-D3 scheme [23] with an empirical damped potential term was added into the energies obtained from exchange–correlation functional in our calculations.

3. Results and discussion

3.1. The physicochemical properties of Ni/SiO₂

The Ni/SiO₂ catalyst prepared by the deposition–precipitation method had a Ni content of 57 wt.% analyzed by AAS, the surface area of 140 m² g⁻¹, and the pore volume of 0.18 cm³ g⁻¹ determined by N₂ adsorption–desorption measurement (Table 1). Shown from SEM image (Fig. 1a), Ni/SiO₂ displayed a blocky texture, with an average particle size of ca. 3 μm. The supported Ni nanoparticles had an average particle diameter of 8.0 nm with a standard deviation of 1.8 nm as determined by TEM image (Fig. 1b), suggesting that the Ni nanoparticles are very uniformly dispersed. The atomic fraction of available Ni atoms on Ni/SiO₂ was 5.0%, as measured by H₂ chemisorption.

3.2. The kinetics and mechanisms for conversion of diphenyl ether in the aqueous phase

3.2.1. The kinetics and reaction pathways of diphenyl ether conversion over Ni/SiO₂

When converting diphenyl ether over metal sites at 393 K, three initial primary routes may exist in the aqueous phase, i.e., hydrog-

Table 1
Physicochemical properties of Ni/SiO₂ catalyst.

Catalyst	Ni/SiO ₂
Metal loading (wt.%)	57
BET surface area (m ² g ⁻¹)	140
Pore volume (cm ³ g ⁻¹)	0.18
Pore diameter (nm)	53
Dispersion (%) (H ₂ chemisorption)	5.0

enolysis of a C–O bond produces equal phenol and benzene, hydrolysis of the C–O bond forms two moles of phenol, and hydrogenation of the aromatic rings to partially hydrogenated products. Shown from the kinetics in Fig. 2a for conversion of diphenyl ether at 393 K in the presence of 0.6 MPa H₂, the initial major products were cyclohexanol, benzene, and cyclohexyl phenyl ether. It is, however, found that phenol was absent from the products although it would be an expected initial product from either the hydrogenolysis or hydrolysis route. It was found in separate experiments that the hydrogenation rate of phenol over Ni/SiO₂ ($130 \text{ mol mol}_{\text{Ni Surf}}^{-1} \text{ h}^{-1}$) was much higher than that of benzene ($2.9 \text{ mol mol}_{\text{Ni Surf}}^{-1} \text{ h}^{-1}$; Table S1), suggesting that the primary phenol was rapidly converted to cyclohexanol [15]. This is consequent to the highly favored adsorption of phenol on the Ni/SiO₂ catalyst, enabling fast hydrogenation to cyclohexanol. Then, the concentration of cyclohexanol should be equal to that of benzene (Scheme 1). But the yield of cyclohexanol kept a constantly stable ratio of 7:3 to benzene, which suggests that besides the hydrogenolysis pathway there is an additional route for cleaving a C–O bond of diphenyl ether.

To understand the intrinsic mechanism and pathways for diphenyl ether C–O bond cleavage, three hypotheses are tested. One was partial hydrogenation forming cyclohexyl phenyl ether, which followed by either hydrogenolysis to produce benzene and cyclohexanol, or hydrolysis to form phenol and cyclohexanol. During diphenyl ether conversion, the yield of partially hydrogenated product increased to a maximum value of 10% at 110 min and then decreased toward zero as reaction time extended. However, in a separate experiment, the rate of cyclohexyl phenyl ether conversion ($0.8 \text{ mol mol}_{\text{Ni Surf}}^{-1} \text{ h}^{-1}$) was much lower than that of diphenyl ether ($26 \text{ mol mol}_{\text{Ni Surf}}^{-1} \text{ h}^{-1}$) at 393 K in the presence of 0.6 MPa H₂ (Table S2). Thus, it is concluded that the partial hydrogenation–hydrogenolysis route is of minor importance. The second route was that diphenyl ether was fully hydrogenated to dicyclohexyl ether, which was fast hydrolyzed to two moles of cyclohexanol. However, in a separate experiment dicyclohexyl ether was completely unreactive over Ni/SiO₂ at 393 K under 0.6 MPa H₂ (Table S2), thus this route can also be ruled out. The third pathway was directly hydrolysis of diphenyl ether to two moles of phenol, and subsequently, phenol was rapidly hydrogenated to cyclohexanol. This would reasonably explain the excess of cyclohexanol.

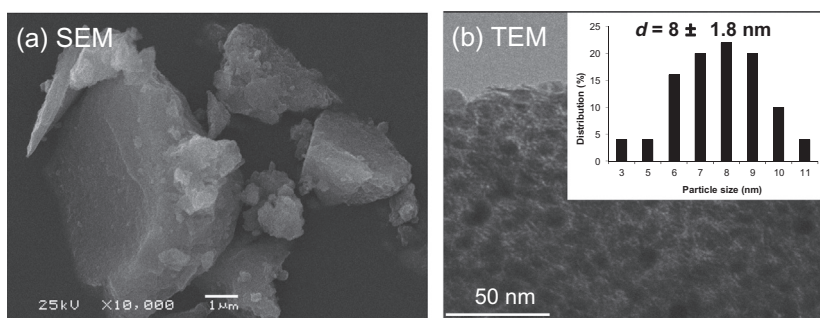


Fig. 1. Characterization of Ni/SiO₂ catalyst (a) SEM, and (b) TEM image and particle size distribution of 300 Ni particles.

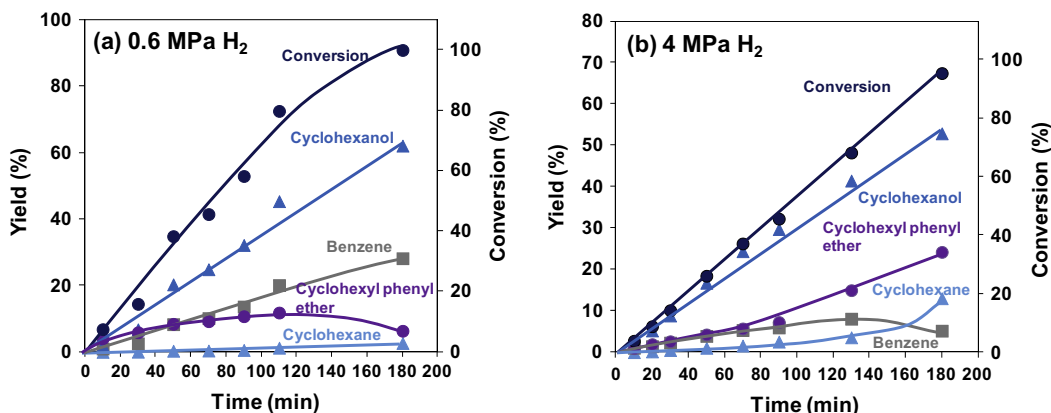


Fig. 2. Diphenyl ether conversion over Ni/SiO₂ in the aqueous phase in the presence of (a) 0.6 MPa H₂ and (b) 4.0 MPa H₂. Reaction conditions: Diphenyl ether (1.70 g), H₂O (80 mL), 57 wt.% Ni/SiO₂ (0.30 g), 393 K, stirring at 700 rpm.

Therefore, we conclude that diphenyl ether is also hydrolyzed to two moles phenol, which is in turn rapidly hydrogenated to cyclohexanol (Scheme 1). Therefore, cyclohexanol is formed by parallel hydrogenolysis–hydrogenation and hydrolysis–hydrogenation pathways. Since the initial yield ratio of cyclohexanol to benzene was 7:3, the rate ratio of hydrogenolysis to hydrolysis routes was determined to be 3:2.

When H₂ pressure was increased from 0.6 MPa (Fig. 2a) to 4.0 MPa (Fig. 2b), the major products remained benzene, cyclohexanol, and cyclohexyl phenyl ether during the diphenyl ether conversion. Phenol was not found due to its rapid hydrogenation rate [24]. The yield of cyclohexyl phenyl ether was increased from 7% to 24% in the presence of the higher H₂ pressure of 4.0 MPa H₂ at 180 min, indicating that the hydrogenation of single aromatic ring of diphenyl ether is favored by the higher H₂ pressure. Cyclohexyl phenyl ether formed could be further cleaved by hydrogenolysis or hydrolysis. At the high hydrogen pressure, fully hydrogenated dicyclohexyl ether was observed with 1% yield at 110 min (not shown in the kinetic curve of Fig. 2b). It was also found that the yield ratio of cyclohexanol to benzene remained 7:3, indicating that the hydrolysis route on DPE persisted under high H₂ pressure. The initial C–O cleavage turnover frequency (TOF) of DPE was calculated from the slope of curves in Fig. 2. In the presence of 0.6 MPa H₂, TOF for diphenyl ether cleavage was 26 mol mol⁻¹_{Ni Surf} h⁻¹, while at higher pressure of 4 MPa it was lowered to 23 mol mol⁻¹_{Ni Surf} h⁻¹. The P_{H2} impact to the C–O bond cleavage rate will be discussed in the following section.

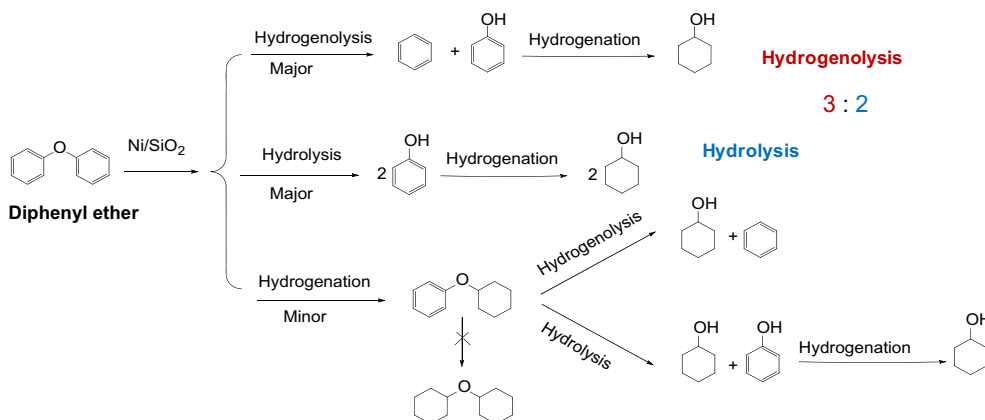
In summary, the conversion of diphenyl ether follows two major reaction pathways (Scheme 1). The first one is that the initial

hydrolysis followed by hydrogenation produces two moles of cyclohexanol. The second one is that hydrogenolysis combined with hydrogenation leads to equivalent moles of benzene and cyclohexanol. There is also a minor reaction pathway, partial hydrogenation (promoted by higher H₂ pressure) followed by hydrogenolysis or hydrolysis produces cyclohexanol and benzene, or cyclohexanol and phenol.

3.2.2. Impact of H₂ pressure

In order to investigate the impact of H₂ pressure (from 0 to 10 MPa) to the C–O bond cleavage TOF, the product distributions from diphenyl ether were recorded at conversions lower than 15% over Ni/SiO₂ at 393 K (Fig. 3a). In the absence of H₂, diphenyl ether did not react indicating that H₂ is required for both hydrolysis and hydrogenolysis routes. Thus, we conclude that for both reaction pathways, the cleavage of the C–O bond is identical in nature and that the difference is primarily related to the availability of H⁺ and OH⁻ and the probability to add to the phenyl radical. With increasing P_{H2}, the TOFs of diphenyl ether C–O bond cleavage increased to the maxima at 0.6 and 1.0 MPa H₂ attaining 26 and 27 mol mol⁻¹_{Ni Surf} h⁻¹, respectively, and then decreased to 17 mol mol⁻¹_{Ni Surf} h⁻¹ at 10 MPa H₂ (Fig. 3a). It also showed that the ether cleavage rate under 0.6 MPa H₂ was higher than that at 4.0 MPa, which is also fitted with the kinetic data in Fig. 2a and Fig. 2b.

Thus, the H₂ competes with the organic reactant for adsorption sites, and the rate-determining step was the C–O bond cleavage on Ni and not adsorption or desorption. Up to medium P_{H2}, the increasing surface coverage by H⁺ leads to an increased hydrogenolysis rate,



Scheme 1. Proposed reaction pathways of diphenyl ether conversion on Ni/SiO₂ in the aqueous phase.

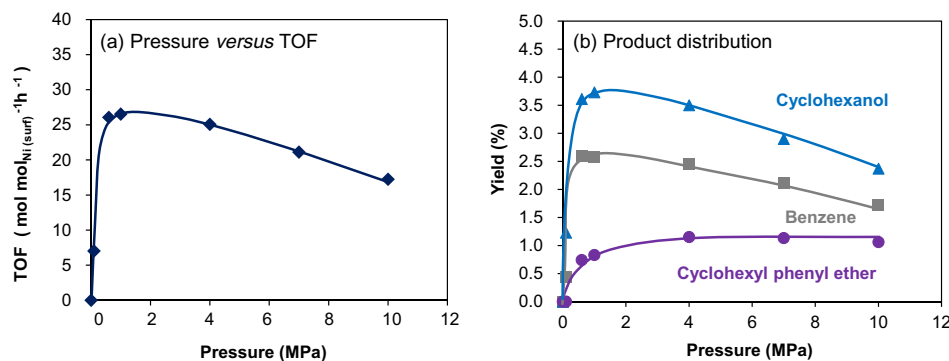


Fig. 3. (a) TOFs for C–O bond cleavage of diphenyl ether over Ni/SiO₂ as a functions of H₂ pressure. Note: TOFs were calculated from the yields of cleaved products at different H₂ pressures. (b) Product distributions from conversion of diphenyl ether (4-O-5) as a function of H₂ pressure. Reaction conditions: diphenyl ether (1.70 g), 57 wt.% Ni/SiO₂ (0.10 g), H₂O (80 mL), 393 K, 30 min., stirring at 700 rpm.

Table 2

Data on C–O bond cleavage of diphenyl ether with Ni-based catalysts.

Catalyst	Conv. (%)	Yield _{C–O cleavage} (%)	Rate _{C–O cleavage} (mol mol _{Ni} ⁻¹ h ⁻¹)	TOF _{C–O cleavage} (mol mol _{Ni Surf} ⁻¹ h ⁻¹)
None	0	0	0	0
SiO ₂	0	0	0	0
Ni/SiO ₂	4.9	4.6	0.30	6.4
Ni/Al ₂ O ₃	2.1	1.8	0.12	5.7
Ni/ZrO ₂	3.1	2.8	0.18	10.5

Conditions: diphenyl ether (1.70 g), H₂O (80 mL), catalyst (20 wt.% Ni, 0.30 g), 393 K, 0.6 MPa H₂, 90 min, stirring at 700 rpm. The Ni dispersions for Ni/SiO₂, Ni/Al₂O₃, and Ni/ZrO₂ were 4.7%, 2.1%, 1.7%, respectively, by H₂ chemisorption.

while at high P_{H_2} , the rate is reduced due to the deficiency of DPE. Fig. 3a represents a typical change in the hydrogenolysis rate of diphenyl ether as a function of hydrogen pressure. With the increase in P_{H_2} , the selectivity for hydrogenated single aromatic ring products increased from 0% to 20% (Fig. 3b), demonstrating that hydrogenation competes with hydrogenolysis on the Ni sites and higher H₂ pressure favored the hydrogenation of a single aromatic ring of diphenyl ether. The cyclohexanol yield increased to a maximum value at 0.6 MPa H₂ and then decreased as P_{H_2} further increased to 10 MPa. In accordance with the earlier observation in the kinetics of diphenyl ether conversion (Fig. 2), the ratio of cyclohexanol to benzene exceeded unity, confirming again the existence of a hydrolysis route for diphenyl ether cleavage.

3.2.3. Impact of catalyst support

To explore the effect of support, 20 wt.% of Ni was supported onto SiO₂, Al₂O₃, or ZrO₂ by the same incipient impregnation method. Reactions were carried out at identical conditions (393 K, 0.6 MPa H₂) for 1.5 h. In the blank tests with no catalyst or SiO₂ in the aqueous phase, diphenyl ether was unreactive at 393 K. Even at 523 K, diphenyl ether was unconverted. In contrast, benzyl phenyl ether was hydrolyzed by the hydronium ions in the water at 523 K [25]. Diphenyl ether was not hydrolyzed because of the C–O bond dissociation energy of diphenyl ether is almost 100 kJ mol⁻¹ higher compared to that of benzyl phenyl ether (314 kJ mol⁻¹ and 218 kJ mol⁻¹, respectively). The yields for diphenyl ether C–O bond cleaved products were 4.6%, 1.8%, and 2.8%, and TOFs were 6.4, 5.7, and 10.5 mol mol_{Ni Surf}⁻¹ h⁻¹ over Ni/SiO₂, Ni/Al₂O₃, and Ni/ZrO₂ catalysts, respectively. The comparable TOFs on three oxides supported Ni catalysts show that these three supports have only a modest effect toward the rates, and the heterogeneous Ni particles on the support were the active sites for cleaving the C–O bond of diphenyl ether (Table 2). In the following work, Ni/SiO₂ was selected as the representative catalyst for further investigation.

3.3. The kinetics and mechanism of conversion of di-*p*-tolyl ether over Ni/SiO₂ in the aqueous phase

p-Dimethyl- and *p*-dihydroxyl-substituted diphenyl ethers were also studied in order to elucidate the influences of the para-substituent on the C–O bond cleavage of diaryl ethers at the selected conditions (393 K, 0.6 MPa H₂). As shown in Fig. 4, 4-methylcyclohexanol and toluene were two major products from di-*p*-tolyl ether conversion. Trace amount of *p*-cresol (yield <1%) was formed during the conversion. Because no partially hydrogenated product was detected, significant aromatic ring hydrogenation prior to di-*p*-tolyl ether scission was excluded. The hydrogenolysis route dominated, producing toluene and *p*-cresol as major products (Scheme 2). Evidently, 4-methylcyclohexanol

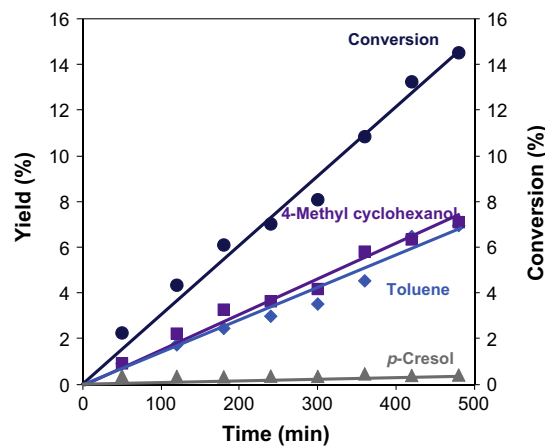
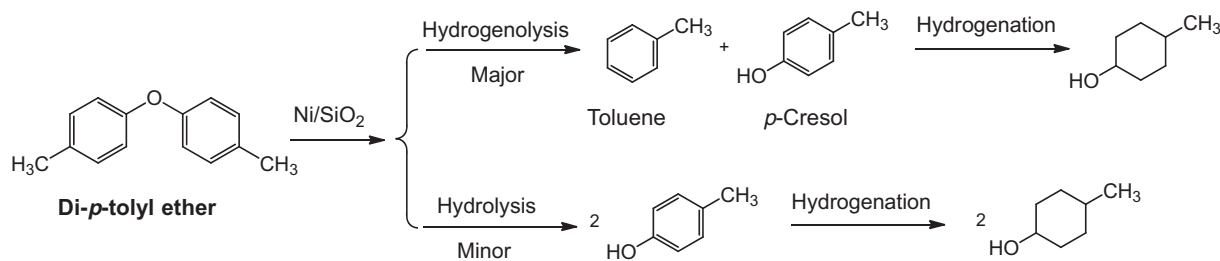


Fig. 4. Di-*p*-tolyl ether conversion over Ni/SiO₂ in the aqueous phase. Reaction conditions: Di-*p*-tolyl ether (1.98 g), H₂O (80 mL), 57 wt.% Ni/SiO₂ (0.30 g), 393 K, 0.6 MPa H₂, stirring at 700 rpm.



Scheme 2. Proposed reaction pathways on di-*p*-tolyl ether conversion on Ni/SiO₂ in the aqueous phase.

was rapidly produced from *p*-cresol hydrogenation over Ni/SiO₂ at same conditions.

To test this hypothesis, a separate experiment with *p*-cresol was carried out over Ni/SiO₂ at 393 K and 0.6 MPa H₂ (Fig. 5). Shown from the plotted conversion data, *p*-cresol was hydrogenated to 4-methyl cyclohexanol with a selectivity exceeding 95%. The hydrogenolysed product toluene was less than 5%. *p*-Cresol was selectively hydrogenated, but not hydrogenolysed, with a rate (TOF = 100 mol mol⁻¹_{Ni Surf} h⁻¹) being two orders of magnitude faster than the rate for cleaving the C–O bond of di-*p*-tolyl ether (1.3 h⁻¹). Thus, 4-methyl cyclohexanol was the major product on di-*p*-tolyl ether conversion. The second point is that Ni/SiO₂ catalyzed not only hydrogenolysis of the C–O bond of di-*p*-tolyl ether, and it catalyzed also the hydrogenation of the aromatic ring of *p*-cresol at identical conditions, demonstrating that hydrogenation and hydrogenolysis were competing on the metal sites. Such competition can be influenced by subtle modifications of the catalytic environment including temperature, pressure, and solvent. Under our conditions, the low temperature and pressure (393 K, 0.6 MPa H₂) favored the selective hydrogenolysis of the C–O bond of diaryl ether, because the hydrogenation rate of the aromatic rings of the phenolic dimer was relatively slow. On the other hand, the energy barrier for the phenolic monomer hydrogenation over Ni sites is much lower [26] than for directly cleaving the phenolic C_{aryl}–OH group [15].

In summary, the C–O bond cleavage of di-*p*-tolyl ether over Ni/SiO₂ at 393 K in the aqueous phase favors a selective hydrogenolysis route, differing from diphenyl ether which is converted by parallel hydrogenolysis and hydrolysis pathways with a rate ratio of 3:2. Di-*p*-tolyl ether is hydrogenolysed over Ni/SiO₂ to produce toluene and *p*-cresol as initial products, and *p*-cresol rapidly hydrogenated to 4-methyl cyclohexanol. TOF of C–O bond cleavage of di-

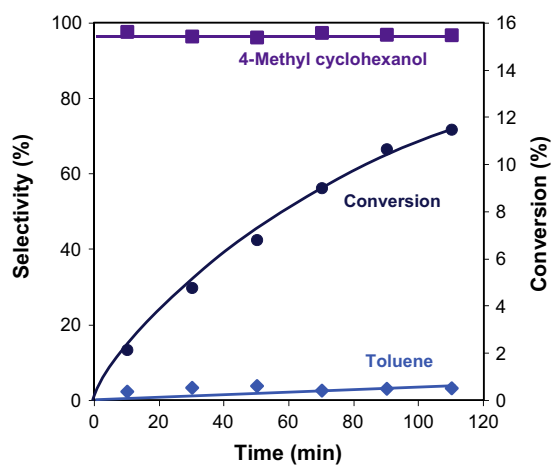


Fig. 5. Kinetics of *p*-cresol conversion over Ni/SiO₂ in the aqueous phase. Reaction conditions: *p*-Cresol (2.16 g), H₂O (80 mL), 57 wt.% Ni/SiO₂ (0.05 g), 393 K, 0.6 MPa H₂, stirring at 700 rpm.

tolyl ether (1.3 mol mol⁻¹_{Ni Surf} h⁻¹) was only one twentieth of diphenyl ether (26 mol mol⁻¹_{Ni Surf} h⁻¹).

3.4. The kinetics and mechanisms of conversion of 4,4'-dihydroxydiphenyl ether over Ni/SiO₂ in the aqueous phase

With conversion of *p*-substituted 4,4'-dihydroxydiphenyl ether at 393 K and 0.6 MPa H₂, the chemistry for breaking the ether C–O bond becomes to be more complex. Phenol, hydroquinone, and single ring hydrogenated products were initial major products. The yield of hydroquinone increased to the maximum of 10% at 40 min and then decreased to 1% at 80 min (Fig. 6). The yield sum of phenol, cyclohexanone, and cyclohexanol increased dramatically with time and exceeded 85% at 80 min. This is difficult to rationalize, because the yield of hydroquinone should be equal to or higher than that of phenol/cyclohexanol (Scheme 3), no matter which route of hydrogenolysis, hydrolysis, or partial hydrogenation–hydrogenolysis it follows. The first and third routes afford equal concentrations of hydroquinone and phenol/cyclohexanol, while the second route provides two moles of hydroquinone. It is presumed that the produced hydroquinone was rapidly hydrogenolysed to phenol, which would lower the hydroquinone concentrations relative to phenol/cyclohexanol. A study on hydroquinone conversion using Ni/SiO₂ was conducted in the aqueous phase at 393 K (Fig. 7).

In the conversion of hydroquinone versus reaction time shown in Fig. 7, the hydrogenated cyclohexane-1,4-dione and cyclohexane-1,4-diol and hydrogenolysis product phenol (Scheme 4) dominated. But three parallel routes might contribute to cyclohexane-1,4-diol formation from hydrogenation of hydroquinone (Scheme 4). The first route is via isomerization to cyclohexene-1,4-dione, followed by sequential hydrogenation to cyclohexane-1,4-dione, 4-hydroxyl cyclohexanone, and cyclohexane-1,4-diol. The second one involves partial hydrogenation to cyclohexa-1,5-diene-1,4-diol, which is isomerized to 4-hydroxycyclohex-2-

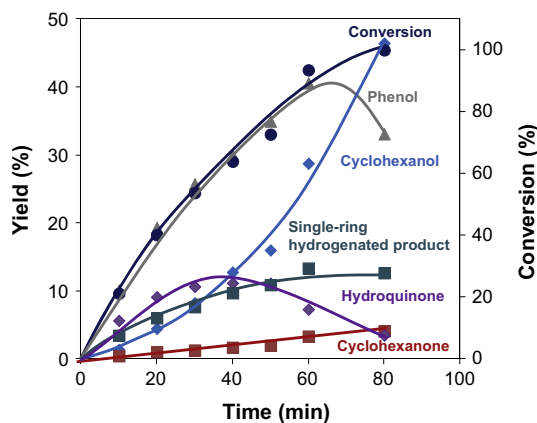
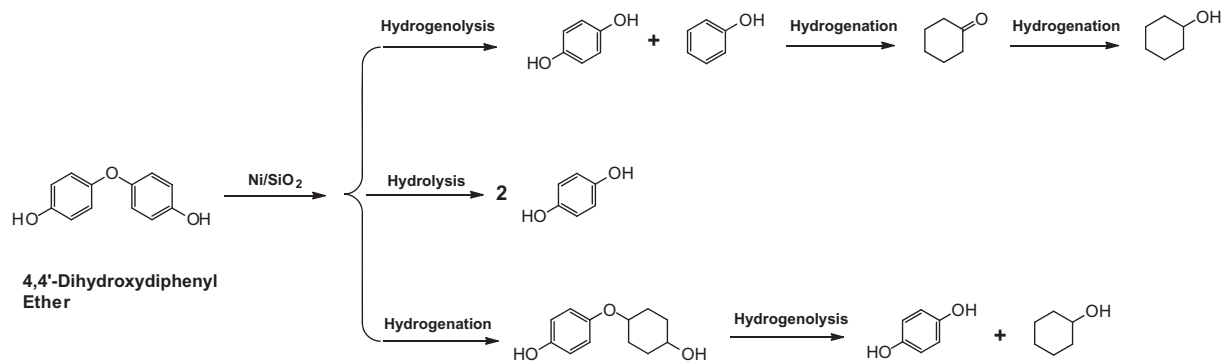


Fig. 6. 4,4'-Dihydroxydiphenyl ether conversion over Ni/SiO₂ in the aqueous phase. Reaction conditions: 4,4'-dihydroxydiphenyl ether (2.02 g), H₂O (80 mL), 57 wt.% Ni/SiO₂ (0.30 g), 393 K, 0.6 MPa H₂, stirring at 700 rpm.



Scheme 3. Proposed reaction pathways of 4,4'-dihydroxydiphenyl ether conversion over Ni/SiO₂ in the aqueous phase.

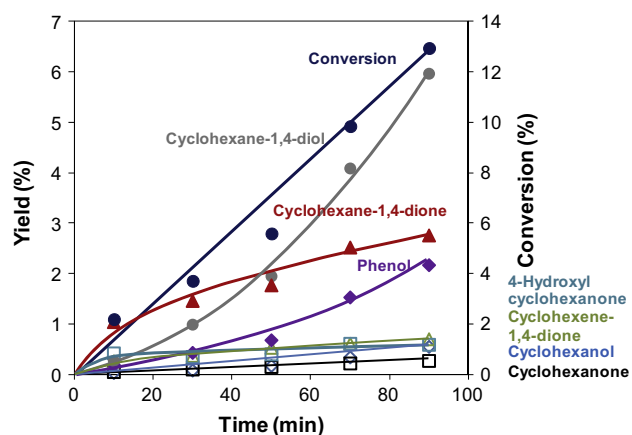


Fig. 7. Hydroquinone conversion over Ni/SiO₂ in aqueous phase. Reaction conditions: Hydroquinone (2.20 g), H₂O (80 mL), 57 wt.% Ni/SiO₂ (0.05 g), 393 K, 0.6 MPa H₂, stirring at 700 rpm.

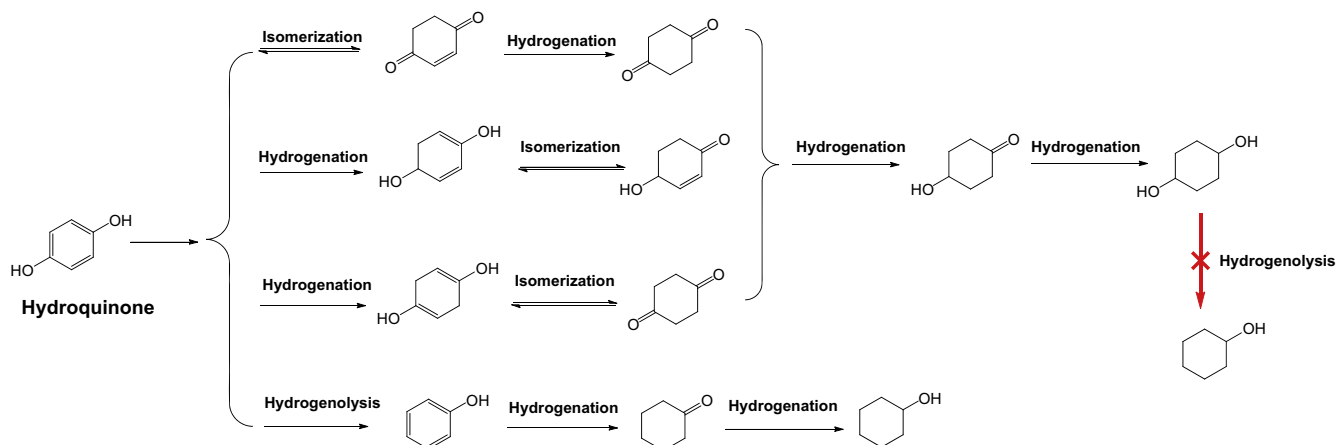
enone, and successive hydrogenation to 4-hydroxyl cyclohexanone and cyclohexane-1,4-diol. The third one includes partial hydrogenation to cyclohexane-1,4-dione-1,4-diol, subsequent isomerization to cyclohexane-1,4-dione, and in turn hydrogenation to 4-hydroxyl cyclohexanone, and cyclohexane-1,4-diol. Since cyclohexane-1,4-dione was the major reaction intermediate during the reaction, the first and third routes were predominant.

It is shown in Fig. 7 that cyclohexane-1,4-dione was converted to cyclohexane-1,4-diol. But the sum of hydrogenolysis yields (3%,

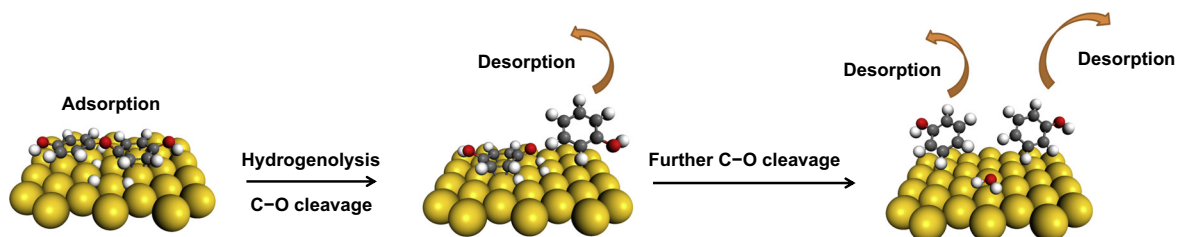
including phenol, cyclohexanol, and cyclohexanone) was lower than one-third of hydrogenation yield (10%, including cyclohexane-1,4-dione, cyclohexane-1,4-diol, cyclohexene-1,4-dione, and 4-hydroxyl cyclohexanone). Hydrogenation of the aromatic ring was the major reaction pathway for hydroquinone, while C–O hydrogenolysis of hydroquinone was minor and hydrogenolysis of cyclohexane-1,4-diol did not occur over Ni/SiO₂ at these conditions. This kinetics study also implies that intermediate phenol via hydrogenolysis of hydroquinone is in a very minor part over Ni/SiO₂ during 4,4'-dihydroxydiphenyl ether conversion.

We infer a mechanism for 4,4'-dihydroxydiphenyl ether conversion on Ni/SiO₂, as shown in Scheme 5. This two-step mechanism involves sequential cleavage of the ether C–O bonds on a metal site. The three O atoms in the adsorbate can be accommodated on the large Ni particle using two Ni sites, and H₂ is also dissociated on the Ni sites. In the second step, the C–O ether bond was cleaved to HOC₆H₄^{*} and OC₆H₄OH^{*} adsorbed on the Ni surface. OC₆H₄OH^{*} adsorbs more strongly than HOC₆H₄^{*} onto the Ni sites due to the two oxygen atoms [27], so that OC₆H₄OH^{*} is retained at the surface and HOC₆H₄^{*} combines with H⁺ to desorb as phenol.

In the surface reaction, OC₆H₄OH^{*} can be further cleaved to phenol and H₂O. Two moles of phenol are thus formed. But during quenching of the batch reactor, OC₆H₄OH^{*} on Ni (1 1 1) may combine with H⁺ to form hydroquinone. The produced hydroquinone intermediate is in a small part converted to cyclohexane-1,4-diol. The adsorbed OC₆H₄OH^{*} is reactive, but the transformation of OC₆H₄OH^{*} to hydroquinone is irreversible. In summary, 4,4'-dihydroxydiphenyl ether is hydrogenolyzed to phenol and OC₆H₄OH^{*} in the first step, and OC₆H₄OH^{*} is further cleaved to phenol and H₂O in the second step.



Scheme 4. Proposed reaction pathways of hydroquinone conversion on Ni/SiO₂ in the aqueous phase.



Scheme 5. Proposed surface reactions on 4,4'-dihydroxydiphenyl ether conversion to two mole phenol and one mole water molecules over Ni/SiO₂.

3.5. DFT modeling results on 4,4'-dihydroxydiphenyl ether conversion over Ni/SiO₂

To test whether the C–O bond cleavage occurred on the surface, DFT calculation was performed on 4,4'-dihydroxydiphenyl ether conversion on the Ni (111) surface. Starting with two H* on the Ni (111) surface, our calculations showed that the most stable adsorption mode for 4,4'-dihydroxydiphenyl ether was co-planar adsorption with both phenolic rings bonding to the surface with an adsorption energy of $-104.9 \text{ kJ mol}^{-1}$ (Fig. 9). As shown in Fig. 9, the first C–O bond scission of 4,4'-dihydroxydiphenyl ether led to the endothermic formation of HOC_6H_4^* and $\text{OC}_6\text{H}_4\text{OH}^*$ intermediates, with a reaction energy change ΔG^0 of $+151.4 \text{ kJ mol}^{-1}$. Then, the $\text{OC}_6\text{H}_4\text{OH}^*$ intermediate was converted to $\text{C}_6\text{H}_4\text{OH}^*$ via the second C–O bond breaking (configurations **b** to **d** in Fig. 8). In addition, the HOC_6H_4^* with H* formed phenol (configurations **b** to **c** in Fig. 8). The calculation indicated that the phenol formation step from HOC_6H_4^* ($-188.6 \text{ kJ mol}^{-1}$) is thermodynamically more favorable than the second C–O bond cleavage step on $\text{HOC}_6\text{H}_4\text{O}^*$

($-122.0 \text{ kJ mol}^{-1}$). This is consistent with our experimental observation in Fig. 6 that phenol is the major initial product in 4,4'-dihydroxydiphenyl ether conversion. In a similar way, hydroquinone ($\text{HOC}_6\text{H}_4\text{OH}$) could also be produced via H* addition to $\text{OC}_6\text{H}_4\text{OH}^*$ intermediate. The formation of hydroquinone was endothermic with ΔG^0 of $+37.0 \text{ kJ mol}^{-1}$ (from -142.1 to $-105.1 \text{ kJ mol}^{-1}$), while the second C–O bond cleavage of $\text{OC}_6\text{H}_4\text{OH}^*$ was less endothermic with ΔG^0 of $+14.9 \text{ kJ mol}^{-1}$ (from -142.1 to $-127.2 \text{ kJ mol}^{-1}$) on the Ni (111) surface. This implies that the formation of hydroquinone is only a minor reaction path in the 4,4'-dihydroxydiphenyl ether conversion (red line in Fig. 9), but the subsequent C–O bond cleavage of $\text{OC}_6\text{H}_4\text{OH}^*$ forming O* and $\text{C}_6\text{H}_4\text{OH}^*$ plays a major role (black line in Fig. 9). Apparently, 4,4'-dihydroxydiphenyl ether undergoes first cleavage of ether C–O bond to form HOC_6H_4^* (phenol precursor), and then, the $\text{OC}_6\text{H}_4\text{OH}^*$ residue suffers C–O bond cleavage to produce $\text{C}_6\text{H}_4\text{OH}^*$ and O* on the Ni/SiO₂ catalyst. This mechanism therefore explains the abundance of phenol (or cyclohexanol) formation from 4,4'-dihydroxydiphenyl ether shown in Fig. 6.

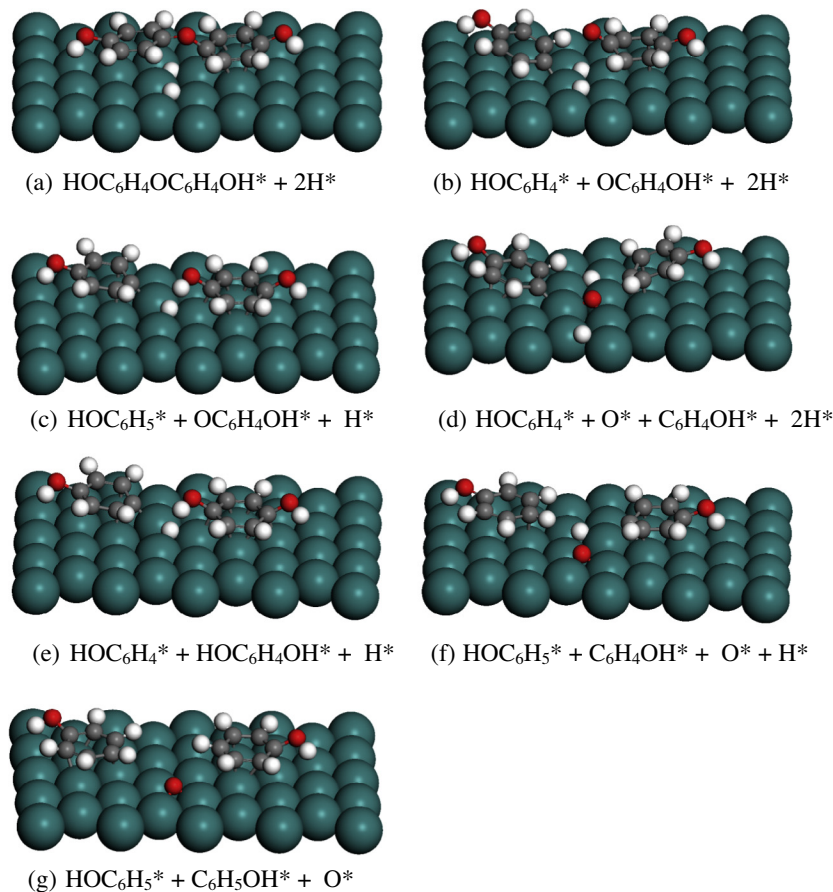


Fig. 8. DFT calculated reaction intermediate configurations in the 4,4'-dihydroxydiphenyl ether conversion on the Ni (111) surface.

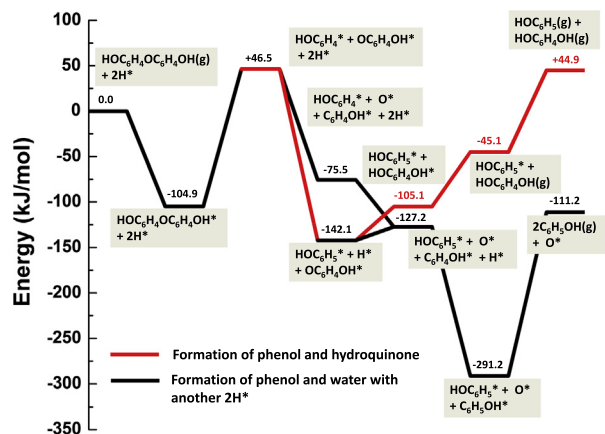


Fig. 9. DFT calculated energy profile of the 4,4'-dihydroxydiphenyl ether conversion on the Ni (111) surface in the presence of atomic hydrogen from H_2 dissociation. The numbers listed in the figure are the energy values relative to the Ni (111) surface with two preadsorbed hydrogen atoms and 4,4'-dihydroxydiphenyl ether in the vacuum.

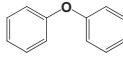
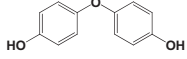
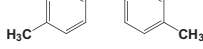
The question now may arise, as to why it was found impossible to cleave the C–O bonds in phenol and *p*-cresol (intermediates from diphenyl ether and di-*p*-tolyl ether conversion) to form benzene and toluene under the reaction conditions chosen. The absence of these products has been rationalized for several reasons. On one hand, the DFT calculated reaction energy of $HOC_6H_5^* \rightarrow C_6H_5^* + OH^*$ is $+124.2 \text{ kJ mol}^{-1}$ (endothermic), which is higher than the phenol adsorption heat of $-93.4 \text{ kJ mol}^{-1}$ on the Ni (111) surface. This suggests that the produced phenol will desorb from the surface instead of undergoing C–O bond scission. On the other hand, the generated $HOC_6H_4^*$, which is formed from the first C–O bond scission of diphenyl ether, will quickly combine with the H^* forming $HOC_6H_5^*$. This step is exothermic (-13 kJ mol^{-1}). In a comparison, the step of $HOC_6H_4^* \rightarrow C_6H_5^* + O^*$ is highly endothermic ($+70.2 \text{ kJ mol}^{-1}$). Therefore, we conclude that benzene formation via the further C–O bond cleavage of phenol or $HOC_6H_4^*$ species is not feasible. Similarly, although the DFT calculated reaction energy of $CH_3C_6H_4OH^* \rightarrow CH_3C_6H_4^* + OH^*$ is less endothermic ($+33.3 \text{ kJ mol}^{-1}$) than the *p*-cresol desorption energy of $+86.5 \text{ kJ mol}^{-1}$, the kinetic activation barrier for the C–O bond-breaking is calculated to be $125.4 \text{ kJ mol}^{-1}$, implying that the *p*-cresol will desorb from the catalyst surface rather than have the C–O bond cleaved. Therefore, based on DFT calculation, benzene and toluene are not expected to be produced by a further cleavage of C–O bond of phenol and *p*-cresol in reactions of di-*p*-tolyl ether and diphenyl ether conversion, which is in good agreement with our experimental results.

3.6. The comparison of initial TOF and E_a of three diaryl ethers over Ni/SiO₂ in the aqueous phase

The initial TOFs and apparent activation energies E_a for C–O bond cleavage are compiled in Table 3. The TOF of 4,4'-dihydroxydiphenyl ether ($69 \text{ mol mol}_{Ni \text{ Surf}}^{-1} \text{ h}^{-1}$) was two times higher than that of diphenyl ether ($26 \text{ mol mol}_{Ni \text{ Surf}}^{-1} \text{ h}^{-1}$). This result agrees well with the observation of Siskin et al. [28] who reported that hydroxyl substituted diphenyl ether was much more reactive than diphenyl ether. This may be because the two hydrophilic hydroxyl groups in 4,4'-dihydroxydiphenyl ether can greatly enhance its solubility in water and the adsorption capability on the metal site [27]. TOF of diphenyl ether ($26 \text{ mol mol}_{Ni \text{ Surf}}^{-1} \text{ h}^{-1}$) was twenty times higher than that of di-*p*-tolyl ether

Table 3

Kinetics data on conversion of three diaryl ethers over 57 wt.% Ni/SiO₂ in the aqueous phase.

Reactant	Initial TOF ^a ($\text{mol mol}_{Ni \text{ Surf}}^{-1} \text{ h}^{-1}$)	E_a (kJ mol^{-1}) ^b
	26	98
	69	93
	1.3	105

^a Initial C–O cleavage rates are obtained from the kinetics data.

^b E_a data are determined from Fig. 10.

($1.3 \text{ mol mol}_{Ni \text{ Surf}}^{-1} \text{ h}^{-1}$). This associates with the fact that hydrophobic methyl group may reduce the solubility of di-*p*-tolyl ether in water and hinder the adsorption on the catalyst surface due to steric effects. Different substituents on diaryl ethers lead to different pathways for cleaving ether C–O bonds over Ni/SiO₂, that is, hydrogenolysis for di-*p*-tolyl ether, hydrogenolysis combined with hydrolysis for diphenyl ether, and sequential surface hydrogenolysis conversion for 4,4'-dihydroxydiphenyl ether. In addition, phenol as the primary product was not observed in diphenyl ether conversion, because the forward phenol hydrogenation rate constant ($13,000 \text{ mol}_{Ni \text{ Surf}}^{-1} \text{ h}^{-1}$) was much faster than the ether cleavage rate constant ($2600 \text{ mol}_{Ni \text{ Surf}}^{-1} \text{ h}^{-1}$) over Ni/SiO₂ in the aqueous phase at 393 K. Phenol, however, appeared in 4,4'-dihydroxydiphenyl ether conversion, as phenol formation rate constant ($13,800 \text{ mol}_{Ni \text{ Surf}}^{-1} \text{ h}^{-1}$) was comparable to the phenol consumption rate constant ($13,000 \text{ mol}_{Ni \text{ Surf}}^{-1} \text{ h}^{-1}$) at identical conditions.

Apparent activation energies are obtained from the Arrhenius plots on three diaryl ether compounds in Fig. 10. TOFs of three diaryl ethers with Ni/SiO₂ in water follow the order of 4,4'-dihydroxydiphenyl ether > diphenyl ether > di-*p*-tolyl ether throughout the range of temperatures examined (353–403 K). The sequence of apparent activation energies (E_a) was 4,4'-dihydroxydiphenyl ether (93 kJ mol^{-1}) < diphenyl ether (98 kJ mol^{-1}) < di-*p*-tolyl ether (105 kJ mol^{-1}).

The apparent activation energy can be expressed by equation [29] (1):

$$E_a^{\text{obs}} = E_a^{\text{true}} + (1 - \theta_A)\Delta H_A + (1 - \theta_B)\Delta H_B \quad (1)$$

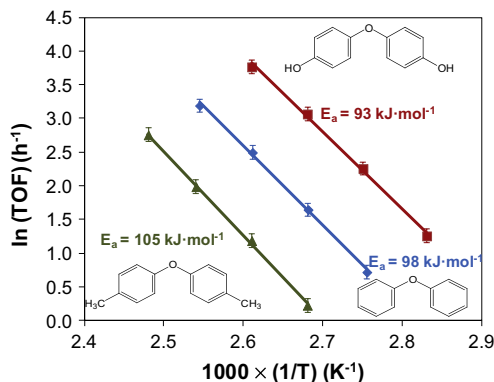


Fig. 10. Arrhenius plots on three diaryl ether compounds at temperature range of 353–403 K. Reaction conditions: H_2O (80 mL), 0.6 MPa H_2 , 57 wt.% Ni/SiO₂ (0.30 g), stirring at 700 rpm, with 4,4'-dihydroxydiphenyl ether (2.02 g) at 10 min; di-*p*-tolyl ether (1.98 g) at 50 min; diphenyl ether (1.70 g) at 50 min.

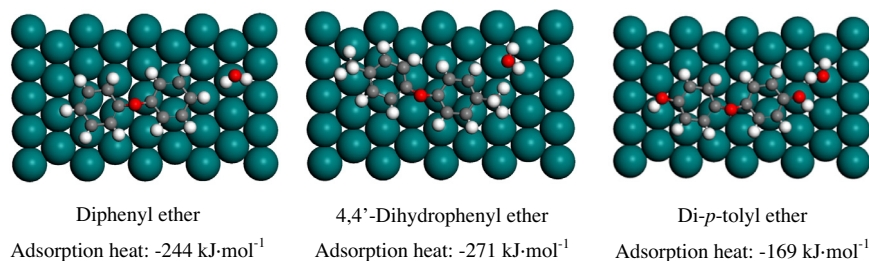


Fig. 11. The energies of adsorption calculated by DFT modeling for adsorbing three ethers and one water molecule onto Ni (1 1 1) surface.

where E_a^{obs} , E_a^{true} , θ_A , θ_B , ΔH_A , and ΔH_B represent the observed activation energy, the true activation energy, the coverage by diaryl ethers, the coverage by H^* , as well as the adsorption heat of diaryl ethers, and adsorption heat of H^* , respectively.

Concerning the range of apparent activation energies, the introduction of an electron donating $-CH_3$ group in para-position slightly strengthens the ether C–O bond, while the addition of the more electronegative $-OH$ weakens the ether C–O bond compared to diphenyl ether. For example, the required energy for breaking C–O bonds of substituted $PhO-CH_3$ follows ($p-CH_3$)- $PhO-CH_3$ (273 kJ mol⁻¹) > $PhO-CH_3$ (268 kJ mol⁻¹) > ($p-OH$)- $PhO-CH_3$ (243 kJ mol⁻¹) [4]. Thus, the C–O bond cleavage barrier (true activation energy) is expected to be in the order E_a^{true} (4,4'-dihydroxydiphenyl ether) < E_a^{true} (diphenyl ether) < E_a^{true} (di-*p*-tolyl ether), on consideration that C–O bond cleavage is the rate-determining step for conversion of three diaryl ethers. On the second point, the $-CH_3$ substitution on diphenyl ether may reduce the heat of adsorption ΔH_A , because steric hindrance and hydrophobic properties of methyl group will decrease the interactions of the aromatic rings of di-*p*-tolyl ether onto Ni (1 1 1) surface in water, while the presence of two $-OH$ groups in 4,4'-dihydroxydiphenyl ether strengthens the interactions with the Ni (1 1 1) surface. Thus, the absolute values of adsorption heats for three ethers on Ni/SiO₂ in the aqueous phase are inferred to decrease in the order $\Delta H_{A,\text{Cal.}}$ (4,4'-dihydroxydiphenyl ether) > $\Delta H_{A,\text{Cal.}}$ (diphenyl ether) > $\Delta H_{A,\text{Cal.}}$ (di-*p*-tolyl ether). Our DFT modeling result strongly supports this hypothesis. It shows that with one water molecule adsorbed, the absolute values of adsorption energies for three ethers on the Ni (1 1 1) surface follow the order $\Delta H_{A,\text{Cal.}}$ (4,4'-dihydroxydiphenyl ether, -271 kJ mol⁻¹) > $\Delta H_{A,\text{Cal.}}$ (diphenyl ether, -244 kJ mol⁻¹) > $\Delta H_{A,\text{Cal.}}$ (di-*p*-tolyl ether, -169 kJ mol⁻¹) (see Fig. 11). With the overall reaction being first order as well as θ_A , θ_B , and ΔH_B being comparable for three ethers, Eq. (1) implies that E_a^{obs} (di-*p*-tolyl ether) > E_a^{obs} (diphenyl ether) > E_a^{obs} (4,4'-dihydroxydiphenyl ether), which is well agreed with the experimental data shown in Fig. 10.

4. Conclusion

A mild route (393 K, 0.6 MPa H₂) for cleaving the ether C–O bonds of three *p*-di-substituted H-, CH₃-, and OH- diphenyl ethers over Ni/SiO₂ has been developed. The choice of SiO₂, Al₂O₃, or ZrO₂ to support the Ni had a small influence on the cleavage rate of the C–O bond of diphenyl ether. The C–O bond of diphenyl ether was cleaved by the parallel hydrogenolysis and hydrolysis routes on Ni sites. The influence of H₂ pressure indicates that the rate-determining step is the C–O bond cleavage but not adsorption or desorption on Ni; thus, the H₂ competed with the organic reactant for adsorption sites which leads to a maximum rate at H₂ pressure of 0.6 MPa at 393 K. In contrast to diphenyl ether, hydrogenolysis was the exclusive route for cleaving the ether C–O bond of di-*p*-tolyl ether producing *p*-cresol and toluene. The sequential surface C–O bond hydrogenol-

ysis contributed to 4,4'-dihydroxydiphenyl ether conversion, that is, it was first cleaved to phenol and OC₆H₄OH*, then further cleaved to phenol (C₆H₄OH* added with H*) and H₂O (O* added with 2 H*) in the second step. DFT calculations confirmed this sequential C–O bond cleavage mechanism of 4,4'-dihydroxydiphenyl ether occurring on the surface of Ni. TOFs of three diaryl ethers with Ni/SiO₂ in water followed the order 4,4'-dihydroxydiphenyl ether (69 mol mol⁻¹_{Ni surf} h⁻¹) > diphenyl ether (26 mol mol⁻¹_{Ni surf} h⁻¹) > di-*p*-tolyl ether (1.3 mol mol⁻¹_{Ni surf} h⁻¹), and in accordance, the sequence of apparent activation energies (E_a) follows 4,4'-dihydroxydiphenyl ether (93 kJ mol⁻¹) < diphenyl ether (98 kJ mol⁻¹) < di-*p*-tolyl ether (105 kJ mol⁻¹). The lowered activation energy for 4,4'-dihydroxydiphenyl ether is attributed to that the presence of two $-OH$ groups strengthens the interaction with Ni (1 1 1) surface, leading to a much lower absolute value of adsorption heat, which is verified by the DFT modeling investigation.

Acknowledgments

J.H. gratefully acknowledges support from the graduate school (Faculty Graduate Center of Chemistry) of the Technische Universität München and the Elitenetzwerk Bayern (graduate school NanoCat). D.M. and J.A.L. acknowledge the support from the US Department of Energy, Office of Basic Energy Sciences, Division of Chemical Sciences, Geosciences & Biosciences. Pacific Northwest National Laboratory (PNNL) is a multiprogram national laboratory operated for DOE by Battelle. Computing time was granted by the grand challenge of computational catalysis of the William R. Wiley Environmental Molecular Sciences Laboratory (EMSL) and by the National Energy Research Scientific Computing Center (NERSC). EMSL is a national scientific user facility located at Pacific Northwest National Laboratory (PNNL) and sponsored by DOE's Office of Biological and Environmental Research.

Appendix A. Supplementary material

Supplementary data associated with this article can be found, in the online version, at <http://dx.doi.org/10.1016/j.jcat.2013.09.012>.

References

- [1] M. Stöcker, *Angew. Chem., Int. Ed.* 47 (2008) 9200.
- [2] W. Boerjan, J. Ralph, M. Baucher, *Annu. Rev. Plant Biol.* 54 (2003) 519.
- [3] J. Zakzeski, P.C.A. Bruijninx, A.L. Jongerijs, B.M. Weckhuysen, *Chem. Rev.* 110 (2010) 3552.
- [4] Y.R. Luo, *Comprehensive Handbook of Chemical Bond Energies*, CRC Press, Boca Raton, FL, 2007.
- [5] E. Furimsky, *Appl. Catal. A* 199 (2000) 147.
- [6] S.H. Townsend, M.A. Abraham, G.L. Huppert, M.T. Klein, S.C. Paspek, *Ind. Eng. Chem. Res.* 27 (1988) 143.
- [7] M. Siskin, A.R. Katritzky, M. Balasubramanian, *Energy Fuels* 5 (1991) 770.
- [8] A.R. Katritzky, R.A. Barcock, M. Balasubramanian, J.V. Greenhill, M. Siskin, W.N. Olmstead, *Energy Fuels* 8 (1994) 487.
- [9] V.M. Roberts, R.T. Knapp, X. Li, J.A. Lercher, *ChemCatChem* 2 (2010) 1407.

- [10] J.M.L. Penninger, R.J.A. Kersten, H.C.L. Baur, *J. Supercrit. Fluids* 16 (1999) 119.
- [11] J.M.L. Penninger, R.J.A. Kersten, H.C.L. Baur, *J. Supercrit. Fluids* 17 (2000) 215.
- [12] X. Wang, R. Rinaldi, *ChemSusChem* 5 (2012) 1455.
- [13] A.G. Sergeev, J.F. Hartwig, *Science* 332 (2011) 439.
- [14] A.G. Sergeev, J.D. Webb, J.F. Hartwig, *J. Am. Chem. Soc.* 134 (2012) 20226.
- [15] J. He, C. Zhao, J.A. Lercher, *J. Am. Chem. Soc.* 134 (2012) 20768.
- [16] C. Zhao, J.A. Lercher, *Angew. Chem., Int. Ed.* 51 (2012) 5935.
- [17] J. VandeVondele, M. Krack, F. Mohamed, M. Parrinello, T. Chassaing, J. Hutter, *Comput. Phys. Commun.* 167 (2005) 103.
- [18] S. Goedecker, M. Teter, J. Hutter, *Phys. Rev. B* 54 (1996) 1703.
- [19] C. Hartwigsen, S. Goedecker, J. Hutter, *Phys. Rev. B* 58 (1998) 3641.
- [20] M. Krack, *Theor. Chem. Acc.* 114 (2005) 145.
- [21] J. VandeVondele, J. Hutter, *J. Chem. Phys.* 127 (2007) 114105.
- [22] J.P. Perdew, K. Burke, M. Ernzerhof, *Phys. Rev. Lett.* 77 (1996) 3865.
- [23] S. Grimme, J. Antony, S. Ehrlich, H. Krieg, *J. Chem. Phys.* 132 (2010) 154104.
- [24] N. Mahata, K.V. Raghavan, V. Vishwanathan, *Catal. Today* 49 (1999) 65.
- [25] J. He, L. Lu, C. Zhao, D. Mei, J.A. Lercher, *J. Catal.*, 2013, <http://dx.doi.org/10.1016/j.jcat.2013.10.024>.
- [26] C. Zhao, S. Kazacov, J. He, J.A. Lercher, *J. Catal.* 296 (2012) 12.
- [27] C. Zhao, Y. Yu, A. Jentys, J.A. Lercher, *Appl. Catal. B* 132–133 (2013) 282.
- [28] M. Siskin, G. Brons, S.N. Vaughn, *Energy Fuels* 4 (1990) 488.
- [29] F. Kapteijn, J.A. Moulijn, R.A. van Santen, R. Wever, *Stud. Surf. Sci. Catal.* 123 (1999) 81.